AN INVESTIGATION OF THE KINEMATIC STRUCTURE OF A TURBULENT FLOW AND THE MOTION OF SOLID PARTICLES IN ITS BOTTOM REGION

N. A. Mikhailova and G. S. Fomenko

Vestnik Moskovskogo Universiteta. Fizika,
Vol. 30, No. 6, pp. 670-678, 1975

UDC 532.529.4

Statistical analysis (based on motion-picture data) of the paths of neutral-buoyancy indicators and heavy particles (mean values and second-order correlation moments for the velocity components) is used to propose a three-layer model of a turbulent flow with solid particles in skipping motion in its bottom region. The presence of a concentration maximum of the solid particles at a fixed distance from the bottom of the flow is explained.

Einstein's probabilistic theory [1] must be acknowledged as most promising for study of the motion of sediment. Papers elaborating on this theory have been published, e.g., [2,3-8]. The experimental studies of [4-13] have refined specific premises of the original versions of the theory or of other theoretical constructions that were also based on the probabilistic approach to description of the mechanism by which bottom sediments move.

Table 1

Characteristics of the Solid Particles

Exper. no.	Particle form factor ψ	Particle size d, cm	Sinking velocity w, cm/sec	Concentration by weight S, %
1	1,060	0,7	14,90	0,46
2	0,975	0,6	11,56	1,08
3	1,240	0,5	14,50	1,58

All three experiments were performed at a Reynolds number $Re = 4.55 \cdot 10^4$, a Froude number Fr = 0.77, a flow gradient i = 0.00635, and a particle density $\rho = 1.31$ g/cm^3.

The present paper reports the results of an experimental study of the motion of solid particles in the bottom region of a turbulent flow. The experiments were performed in a trough 7 m long, 20 cm wide, and 40 cm high. Roughness was created by polystyrene foam balls (1 cm in diameter), which were cemented to glass plates. The liquid discharge was determined at a triangular weir and calculated from the average-velocity curve obtained by processing the statistical material. External sediment saturation of the flow was used. The total solid-particle concentration was determined by the ratio of the solid to the liquid flowrates. Three experiments were performed with different solid-particle saturations of the flow. The sediment characteristics are given in Table 1.

The form factor of the particles was determined from the formula $\psi = \frac{\pi D^2}{4S}$, where D is the diameter of the sphere of equal volume and S is the area of the particle's largest cross section. It was established on determination of the settling velocity that the manner in which the particles settle in the standing water varies sharply with changes in the form factor: the closer the shape of the particle to spherical, the more nearly rectilinear is its path; in the case $0{,}6 \leqslant d < 0{,}7$ cm, for which the shape is closer to lamellar, the path can be described as stepped; here the fall time of the particle increases and its sinking velocity decreases.

Motion-picture photography was used to investigate the kinematic structure of the flow and the behavior of the particles in it [9,10]. The "Konvas" camera was set up beside the trough at a distance of 1 m from it; two 1000-watt lamps were used for top-slit lighting with a slit width of 2.5 cm and an illuminated strip width of 3.5 cm on the bottom of the flow. In accordance with [14], the possible perspective errors were determined from the formula

$$\Delta l = \frac{\delta y}{an + y},$$

where Δl is the perspective distortion, a is the distance of the lens from the wall of the trough, δy is the change in particle distance during exposure, n is the refractive index of the water, and y is the distance from the trough wall to the center of the illuminated strip in the flow. In our experiments, a = 1 m, n = 1.33, y = 10 cm, δy = 1.75 cm, and Δl did not exceed 1.23%.

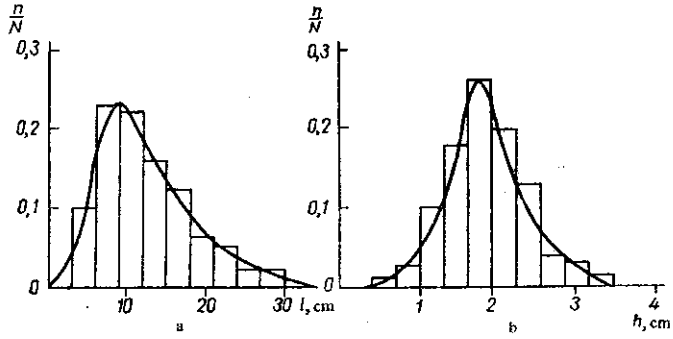

Fig. 1. Distribution curves of lengths (a) and heights (b) of "skips" by solid particles.

The indicator used was an acrylate powder with a density close to that of water and particle diameters of ~1 mm. The film frames were processed on a "Mikrofot" 5 PO-1 projection-type unit fitted with a moving coordinate frame. The reading accuracy was 0.05 mm, and the time between two successive records of the indicator particles was 0.026 sec.

The paths of the particles moving in the flow were reduced as follows. A particle entering the frame was picked up on the card and its motion was followed until it left the field; the positions of the particle were marked on the card for each frame, two successive positions of the particle on the card being separated by t = 0.052 sec. The subsequent processing of the paths was done on the projector unit. The card was held in a fixed position, and the scale was moved relative to it.

In experiment 1, 93 cards carrying records of 3000 particle displacements were processed. Analysis of the paths showed that most of them are characterized by a steep rise and a much gentler descent. Figure 1 shows the distributions of the skip lengths and heights. The skip-length distribution can be described by a Pearson curve of type II [11]. The skip-height distribution is much more symmetrical. The manner in which the particles move is strongly influenced by their rotation, which is easily followed on the recorded paths. What occurs is a rotation in three dimensions in which the image plane of the particle being projected onto the screen and the angle between the largest particle diameter and the bottom mark of the flow vary through wide ranges. Saltation is also accompanied by a transition to the suspended state: in its descent, the particle "is not allowed" to settle onto the bottom, but is caught up by an eddy and begins a new ascent, with the result that the skip length increases considerably. Skips up to 33 cm long, or 14 times the ascent height, were observed in experiment 1. This type of particle motion is due either to transport of the particle by large-scale structural formations [11] or to the influence of small eddies that arise downstream of roughness projections. The importance of the respective factors can be decided on the basis of study of the Lagrangian correlation functions.

A BESM-4 computer was used for statistical reduction of the experimental data. The data-processing program included a computation of estimates for the mean values, variances, rms deviations, skewness, and excess. The conversion from the particle displacements determined on screen projection of the film to the velocity characteristics of the flow was made with the formulas

$$\bar{u} = \frac{k\Sigma\Delta x_i}{\tau n}, \quad \bar{v} = \frac{k\Sigma\Delta y_i}{\tau n},$$

where $\bar{u}$ and $\bar{v}$ are the longitudinal and vertical flow and particle velocities, Δx_i and Δy_i are the horizontal and vertical displacements, n is the number of particles in the zones into which the flow picture is divided along the vertical, t is the time between two successive records of indicators or particles, τ is the filming scale, which equals the ratio

of the distance between the stationary markers to the distance between their images on the frame;

$$\sigma_u = \frac{k}{\tau}\sqrt{\overline{\Delta x^2} - \overline{(\Delta x)^2}} \quad \text{and} \quad \sigma_v = \frac{k}{\tau}\sqrt{\overline{\Delta y^2} - \overline{(\Delta y)^2}},$$

where σ_u and σ_v are the rms deviations of the longitudinal and vertical flow and particle velocity components;

$$\overline{u'v'} = (\overline{\Delta x\,\Delta y} - \overline{\Delta x}\,\overline{\Delta y})\frac{k^2}{\tau^2},$$

where $\overline{u'v'}$ is the moment of the correlation between the instantaneous values of the horizontal and vertical velocity components (calculated for the flow and the particles);

$$D_u = \sigma_u^2 \quad \text{and} \quad D_v = \sigma_v^2,$$

where D_u and D_v are the variances of the longitudinal and vertical velocity components for the flow and the particles;

$$k_n = \frac{\overline{u'v'}}{\sigma_u \cdot \sigma_v},$$

where k_n is the normalized correlation coefficient.

The skewness and excess were calculated from the formulas

$$S_k = \frac{\mu_3}{\sigma^3}, \quad E_x = \frac{\mu_4}{\sigma^4} - 3,$$

where μ_3 and μ_4 are the third and fourth central moments.

The confidence intervals for the average velocities were calculated from the formulas

$$\varepsilon_\beta = \sqrt{\frac{\tilde{D}}{n}}\, t_\beta,$$

where $\tilde{D}$ is the estimated variance for the particular zone, n is the number of independent values, and $t_\beta = \sqrt{2}\,\Phi^{-1}(\beta)$, where $\Phi^{-1}(\beta)$ is the inverse Laplace function.

The confidence intervals ε_{β_D} for the variances were determined as

$$\varepsilon_{\beta_D} = \sqrt{\frac{2}{n-1}}\,\tilde{D}\, t_\beta,$$

and those for the rms deviations, $\varepsilon_{\beta_\sigma}$, from the formula

$$\varepsilon_{\beta_\sigma} = \sqrt{\varepsilon_{\beta_D}}.$$

For our fiducial probability $\beta = 0.67$, we have $t_\beta = 1$.

Analysis of curves of the average longitudinal flow velocity component values indicates that as the saturation of the flow with sediment increases (Fig. 2a), the area of the diagram decreases, with a substantial change in the velocity gradient near the bottom (Fig. 2b). There is an apparent increase in the liquid flowrate, which may be due to occupation of much of the clear cross section by solid particles at high saturations of the flow. This effect is most pronounced in experiment 3, where the saturation S = 1.58%.

The intensity of the turbulence in the bottom region decreases with increasing particle saturation of the flow (Fig. 2a, curves 3, 4, and 5). In the case of heavy saturation (experiment 3), the vertical distribution of turbulent intensity changes considerably. Instead of the usual maximum at a relative distance $\eta = 0.2$ from the bottom of the flow, we have a conspicuous maximum at a relative distance $\eta = 0.4$. This can also be explained by the presence of the layer heavily saturated with solid particles in the bottom region. Turbulent fluctuations are extinguished in this layer, which has a rather well-defined boundary. Its upper boundary is a kind of bottom for the flow. Although the conditions of solid-particle penetration from this layer into higher layers have not yet been

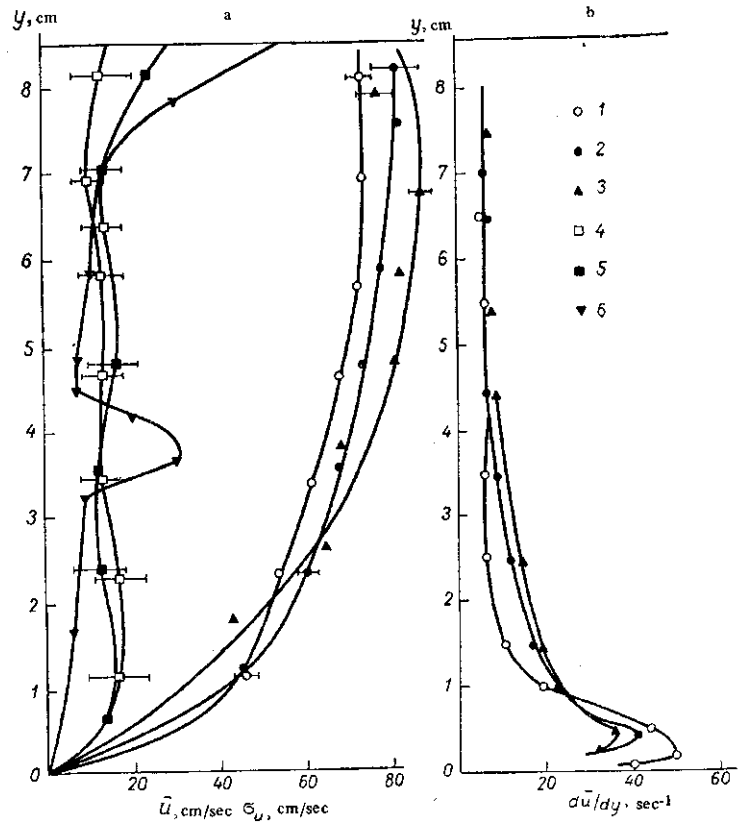

Fig. 2. Vertical distributions of average velocity values (a, curves 4, 5, 6) and average-velocity gradient (b, curves 1, 2, 3) for experiments 1, 2, and 3, respectively.

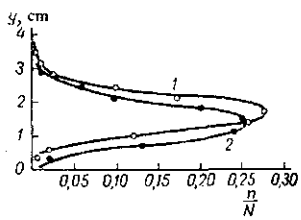

Fig. 3

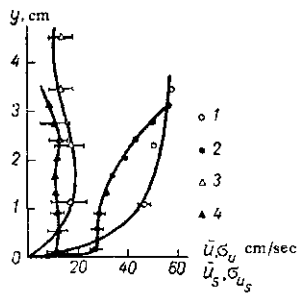

Fig. 4

Fig. 3. Vertical distributions of probabilities that the particle will be on the ascending (1) and descending (2) trajectory branches.

Fig. 4. Vertical distributions of average velocity values (1, 2) and rms deviations of horizontal velocity component (3, 4) for the flow and solid particles, respectively.

investigated, it is obvious that they must differ significantly from the conditions for separation of particles from the bottom of the flow. At the surface of the flow, a sharp increase in turbulent intensity is observed for all three saturation levels, and can be explained by friction at the water-air interface at the comparatively large Froude numbers.

For experiment 1, we investigated the probability density distribution of given solid-particle heights above the bottom. In Fig. 3, curve 1 corresponds to cases of ascending particle motion and curve 2 to descending motion. These curves can be regarded as

approximate concentration curves of a sort. Since particle concentration is proportional to the probability that the particles will be at a given height, it can be concluded that the concentration maximum occurs not at the bottom of the flow, but at a certain height $\eta = 0.2$ above the bottom.

Table 2

Test of Satisfaction of Normal Distribution Law for Instantaneous Flow and Solid Particle Velocities (Experiment 1)

№	Zone	Sample vol., n	Skewness for U, S_{k_u}	Skewness for V, S_{k_v}	$3\sigma_{S_k}$	Excess for U, E_{x_u}	Excess for V, E_{x_v}	$5\sigma_{E_k}$
			Flow					
1	$0{,}57 \leqslant y_1 < 1{,}74$	56	0,59	0,96	0,99	0,42	1,53	2,84
2	$1{,}74 \leqslant y_2 < 2{,}91$	100	0,18	—0,47	0,78	—0,05	1,63	2,28
3	$2{,}91 \leqslant y_3 < 3{,}09$	100	—0,12	0,40	0,78	0,08	2,21	2,28
4	$3{,}09 \leqslant y_4 < 5{,}25$	125	1,48	0,02	0,66	8,24	0,79	2,02
5	$5{,}25 \leqslant y_5 < 6{,}42$	133	—0,08	0,06	0,63	1,67	1,20	1,96
6	$6{,}42 \leqslant y_6 < 7{,}59$	191	0,21	0,51	0,53	4,79	6,43	1,77
7	$7{,}59 \leqslant y_7 < 8{,}50$	33	—0,33	0,17	2,70	2,51	0,15	3,40
			Solid particles					
1	$0 \leqslant y_1 < 0{,}37$	41	0,43	—4,04	1,07	—0,37	18,47	3,20
2	$0{,}37 \leqslant y_2 < 0{,}75$	108	0,41	1,00	0,71	—0,34	—0,78	2,37
3	$0{,}75 \leqslant y_3 < 1{,}13$	515	0,55	0,36	0,32	0,44	1,76	0,11
4	$1{,}13 \leqslant y_4 < 1{,}50$	906	0,41	—1,84	0,24	0,00	20,55	0,81
5	$1{,}50 \leqslant y_5 < 1{,}87$	765	0,32	—17,09	0,27	—0,37	360,04	0,87
6	$1{,}87 \leqslant y_6 < 2{,}25$	415	0,30	—15,40	0,36	—0,41	283,86	1,20
7	$2{,}25 \leqslant y_7 < 2{,}63$	132	—0,32	0,03	0,63	—0,98	0,38	2,00
8	$2{,}63 \leqslant y_8 < 2{,}00$	27	0,07	0,30	1,29	—0,13	—0,37	3,60
9	$3{,}00 \leqslant y_9 < 3{,}37$	19	—1,33	1,00	1,48	1,72	0,48	3,84

For a nondeformable bottom, it follows from the continuity equation for the property being transported that

$$\overline{V_{s_1} S_1} = \overline{V_{s_2} S_2},$$

where V_{s_1} and S_1 are the instantaneous values of the vertical velocity component and the particle concentration at the bottom of the flow and V_{s_2} and S_2 are the instantaneous values of the vertical velocity component and concentration at the boundary surface corresponding to the maximum probability that the particles will rise to a given height.

If V_{s_1} decreases significantly near the upper boundary of the sediment-saturated layer (as a result of decay of the eddies formed at the bottom), S_2 should increase, since the above equality must be preserved. Hence it follows that the solid-particle concentration maximum should occur at a certain distance from the bottom of the flow that is determined by the conditions of eddy decay and the sinking rate of the solid particles. The results obtained suggest that the sediment-laden flow consists of three layers: an upper layer, which occupies most of the depth of the flow and to which penetration of solid particles is improbable, a thin layer with the highest concentration, and a sediment-poor bottom layer.

Statistical processing of the films indicated that the skipping heavy particles lag behind the liquid (Fig. 4, curves 1 and 2). The same result had been obtained earlier [11] for particles suspended in a flow. However, the velocity difference was observed to increase with distance from the bottom for suspended sediment, while in our case the lag becomes smaller as the rise height of the particles increases. The rms deviations of the longitudinal velocity component decrease both for skipping particles (Fig. 4, curves 3 and 4) and for suspended sediment [11].

The vertical velocity component is small and usually negative. This can be explained by the high sinking velocity of the particles (see Table 1); the maximum values of the vertical velocity component also correspond to the maximum of the rms deviation.

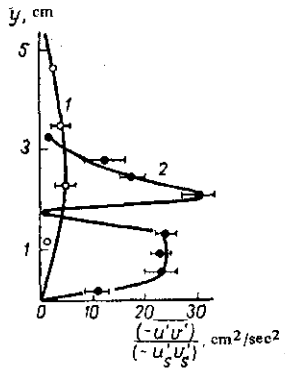

Fig. 5. Vertical distributions of moments of correlation between horizontal and vertical velocity components for the flow (1) and the solid particles (2).

Table 2 gives the values of the skewness S_k and excess E_x for the flow and the particles. Normality of the distribution of the instantaneous velocity values was tested by the method of moments [15], which is based on satisfaction of the inequalities

$$|S_k| \leqslant 3\sigma_{S_k}, \quad |E_x| \leqslant 5\sigma_{E_x},$$

for the normal distribution; here δ_{S_k} is the rms deviation of the skewness S_k and δ_{E_x} is the rms deviation of the excess E_x;

$$\sigma_{S_k} = \sqrt{\frac{6(n-1)!}{(n+1)(n+3)}}, \quad \sigma_{E_x} = \sqrt{\frac{|24n(n-2)\cdot(n-3)}{(n+1)^2(n+3)(n+5)}},$$

where n is the number of independent values in the sample.

It follows from analysis of Table 2 that the normal distribution law is satisfied everywhere except in zone 4 for the instantaneous values of the longitudinal flow velocity component, and that for the vertical component it is also violated near the surface, an effect that can be explained by friction at the water-air boundary. For the solid particles, the instantaneous longitudinal velocities are normally distributed everywhere except in zone 3, which is adjacent to the region of maximum sediment saturation of the flow. The normal distribution does not apply for the vertical velocity component of the solid particles, since there is a factor in constant operation—the force of gravity, under whose action the particles are in fall at every instant of time.

Figure 5 (curves 1, 2) shows the vertical distribution of the correlation moments $\overline{u'v'}$ for the liquid and $\overline{u'_s v'_s}$ for the solid particles. We observe a decrease in the correlation coefficient for the solid particles to a near-zero value at the height $\eta = 0.2$, the height of maximum probability for the particles (see Fig. 3), while no such variation of $\overline{u'_s v'_s}$ is observed for particles suspended in the core of the flow [16]. This phenomenon is easily explained by the three-layer flow model examined above.

In conclusion, one explanation can be offered for the mechanism of particle motion in the bottom layer. Large-scale eddies determined by the geometry of the flow are responsible for particle transport in the direction of the flow. Evidently, the skipping length is determined by the conditions of motion of these large-scale structural formations and is related to the characteristic period of the Lagrangian correlation function. The actual separation of the particles from the bottom is correctly determined by Einstein [1] and M. A. Velikanov [2] from the condition that the lifting force exceed the force of gravity, whence follows the inequality $U_{cr} \geqslant C\sqrt{gD}$ for determination of the critical velocity; here C is a coefficient that depends on the shape and density of the particles, D is the particle diameter, and g is the acceleration of gravity. Thus, the separation conditions are determined by the fluctuation characteristics of the horizontal velocity component. On the other hand, suspension of the particles, which determines their motion in the vertical plane, occurs under the action of smaller eddies that are determined by the roughness of the bottom and the velocity gradient at the bottom.

REFERENCES

1. H. A. Einstein, Proc. Amer. Soc. Civ. Eng., vol. 7, 1941.
2. M. A. Velikanov, Dynamics of Channel Flows, Vol. II, Sediment and the Bed [in Russian], Moscow, 1955.
3. K. I. Rossinskii, Trudy Gos. Gidrol. In-ta, no. 160, 1968.
4. K. I. Rossinskii and K. S. Lyubomirova, Trudy Gos. Gidrol. In-ta, no. 162, 1969.
5. Y. Tsuchiya, "Proc. Fifteenth Congr. Intern. Ass. Hydr. Research," vol. 2, 1969.

6. N. A. Mikhailova, M. M. Arkhangel'skii, V. S. Verbitskii, and Z. Sh. Klyusek, "A probabilistic scheme of motion of solid particles in the bottom region of a turbulent flow," Abstracts of Papers at Lomonosov Lectures [in Russian], Moscow, 1970.
7. K. I. Rossinskii and K. S. Lyubomirova, in collection: Dynamics and Thermics of River Flows [in Russian], Moscow, 1972.
8. T. E. Mirtskhoulava, A. V. Magomedova, et al., Proc. Fifteenth Congr. Intern. Ass. Hydr. Research, vol. 1, 1973.
9. N. A. Mikhailova, Izv. AN SSSR. Mekh., mashinostr., no. 10, 1952.
10. N. A. Mikhailova, Izv. AN SSSR. Mekh. i mashinostr., no. 4, 1962.
11. N. A. Mikhailova, Transport of Solid Particles by Turbulent Water Flows [in Russian], Leningrad, 1966.
12. S. K. Olevinskaya, A. A. Pivovarov, and K. I. Rossinskii, Vodnye resursy, no. 2, 1973.
13. K. M. Arbulieva, S. K. Olevinskaya, and A. A. Pivovarov, Vestn. Mosk. un-ta. Fizika [Moscow University Physics Bulletin], vol. 14, no. 3, 1973.
14. B. A. Fidman, Trudy Gos. Gidrol. In-ta, no. 160, 1968.
15. E. I. Pustyl'nik, Statistical Methods for the Analysis and Reduction of Observations [in Russian], Moscow, 1968.
16. G. A. Dmitrieva, in collection: Problems of Hydraulics [in Russian], no. 2, 1970.

17 June 1974

Department of the Physics of the Sea and Inland Waters